

CH₃-Terminated Carbon Chains in the GOTHAM Survey of TMC-1: Evidence of Interstellar CH₃C₇N

MARK A. SIEBERT,¹ KIN LONG KELVIN LEE,² ANTHONY J. REMIJAN,³ ANDREW M. BURKHARDT,^{4,5}
THE GOTHAM COLLABORATION,³ RYAN A. LOOMIS,³ MICHAEL C. MCCARTHY,⁴ AND BRETT A. MCGUIRE^{2,3,4}

¹*Department of Astronomy, University of Virginia, Charlottesville, VA 22904, USA*

²*Department of Chemistry, Massachusetts Institute of Technology, Cambridge, MA 02139, USA*

³*National Radio Astronomy Observatory, Charlottesville, VA 22903, USA*

⁴*Center for Astrophysics | Harvard & Smithsonian, Cambridge, MA 02138, USA*

⁵*Department of Physics, Wellesley College, 106 Central Street, Wellesley, MA 02481, U.S.A.*

(Accepted October 20, 2021)

Submitted to ApJ

ABSTRACT

We report a systematic study of all known methyl carbon chains toward TMC-1 using the second data release of the GOTHAM survey, as well as a search for larger species. Using Markov-Chain Monte Carlo simulations and spectral line stacking of over 30 rotational transitions, we report statistically significant emission from methylcyanotriacetylene (CH₃C₇N) at a confidence level of 4.6 σ , and use it to derive a column density of $\sim 10^{11}$ cm⁻². We also searched for the related species, methyltetraacetylene (CH₃C₈H), and place upper limits on the column density of this molecule. By carrying out the above statistical analyses for all other previously detected methyl-terminated carbon chains that have emission lines in our survey, we assess the abundances, excitation conditions, and formation chemistry of methylpolyynes (CH₃C_{2n}H) and methylcyanopolyynes (CH₃C_{2n-1}N) in TMC-1, and compare those with predictions from a chemical model. Based on our observed trends in column density and relative populations of the *A* and *E* nuclear spin isomers, we find that the methylpolyynes and methylcyanopolyynes families exhibit stark differences from one another, pointing to separate interstellar formation pathways, which is confirmed through gas-grain chemical modeling with *nautilus*.

Keywords: Astrochemistry, ISM: molecules

1. INTRODUCTION

One of the most well-studied sites of cold, interstellar carbon chemistry is a prestellar core within the Taurus Molecular Cloud complex commonly referred to as Taurus Molecular Cloud 1 (TMC-1) (Churchwell et al. 1978). The chemistry occurring in TMC-1 produces a suite of exotic molecules (by terrestrial standards) including unsaturated cyanopolyynes (HC_{2n+1}N; $n = 1, 2, 3, \dots$) and acetylenic (C_{2n}H₂) linear carbon chains. Among the variations on these abundant molecules are the symmetric top methylpolyynes (MPs) and methylcyanopolyynes (MCPs), which have the form CH₃C_{2n}H and CH₃C_{2n-1}N, respectively. These species have been known in the interstellar medium (ISM) since the dis-

covery of methyl cyanide (CH₃CN) (Solomon et al. 1971) and methyl acetylene (CH₃CCH) (Irvine et al. 1981). Toward TMC-1, methylpolyynes and methylcyanopolyynes as large as CH₃C₆H and CH₃C₅N have been detected and characterized (Matthews & Sears 1983; Irvine et al. 1981; Broten et al. 1984; Walmsley et al. 1984; MacLeod et al. 1984; Loren et al. 1984; Snyder et al. 2006; Remijan et al. 2006).

Currently, the chemical formation of MPs and MCPs in TMC-1 is unconstrained. While it is possible that simple carbon addition reactions occurring on the surfaces of dust grains may account for the growth of these species toward cold, dark clouds (Turner et al. 2000), it is also plausible that ion-molecule reaction pathways in the gas phase can account for their formation (Quan & Herbst 2007). Because molecules with C_{3v} symmetry have unique excitation properties that do not allow for easy interconversion between *A* and *E* symme-

try states, the relative populations of their K -ladders can offer additional clues to their formation conditions (see e.g. Minh et al. (1993) Askne et al. (1984), Willacy et al. (1993), (Mendoza et al. 2018)), but to date, analysis of these populations has only been done for the shortest MPs and MCPs. Furthermore, comparing the relative column densities of the similarly structured cyanopolyynes has proven to be a useful tool in testing chemical models and assessing the mechanisms through which carbon chain species grow in the ISM (Loomis et al. 2021; Agúndez et al. 2017; Burkhardt et al. 2018).

Obtaining a more complete understanding of their chemistry and setting constraints on the abundances and excitation conditions of the various methyl-terminated carbon chains requires exploring the extent to which these types of species can grow (i.e. how long of a C-chain can form). Such observations would enable the direct comparison of measured abundances with both grain-surface and gas-phase reaction pathways, especially when combined with a fully self-consistent excitation analysis of MPs and MCPs in TMC-1. In addition, these studies will set the overall limit to the detectability of longer chain MPs and MCPs based on both an improved understanding of the chemical formation pathway and on a new computational methodology to detect the weak signals coming from the larger C-chain species.

The ongoing GOTHAM survey (GBT Observations of TMC-1: Hunting for Aromatic Molecules) along with a deep Q-band survey being conducted on the Yebes 40 m radio telescope (Cernicharo et al. 2020) have thus far proven to be very useful for rigorous studies of exotic molecules in TMC-1. With many new detections of various carbon-bearing molecules, their isomers, and cyclic/polycyclic species, these projects have effectively expanded our knowledge of the interstellar molecular carbon reservoir before star formation occurs (Xue et al. 2020; Loomis et al. 2021; McGuire et al. 2018; McCarthy et al. 2020; McGuire et al. 2020; McGuire et al. 2021; Cabezas et al. 2021; Cernicharo et al. 2021). In this work, we present a detailed analysis of CH_3 -terminated carbon chains toward TMC-1 as well as the first detection of methylcyanotriacetylene ($\text{CH}_3\text{C}_7\text{N}$, Chen et al. (1998)) using the second data release of GOTHAM. We also search for methyltetraacetylene ($\text{CH}_3\text{C}_8\text{H}$, Travers et al. (1998a)) in our data, but do not find significant emission and thus report upper limits on its abundance.

In Section 2, we outline the specifics of our observations and reduction methods. In Section 3 we describe our spectroscopic calculations for the targeted molecules and statistical analysis procedures. In Section 4 we present our results for all targeted molecules and discuss

their relative column densities and excitation physics. Finally, in Section 5 we discuss how our results fit in to the current understanding of chemistry in TMC-1, and compare them with predictions of our chemical model.

2. OBSERVATIONS

Observations obtained in this study were collected as part of the GOTHAM Survey. GOTHAM is a large project on the 100m Green Bank Telescope (GBT) currently carrying out dedicated spectral line observations of TMC-1 covering almost 30 GHz of radio bandwidth at high sensitivity and ultra-fine spectral resolution. This work uses the second data release (DR2) of GOTHAM, which includes over 600 hours of observations targeting the cyanopolyyne peak (CP) of TMC-1, centered at $\alpha_{\text{J2000}} = 04^{\text{h}}41^{\text{m}}42.5^{\text{s}}$, $\delta_{\text{J2000}} = +25^{\circ}41'26.8''$. A full description of DR2 specifications and our reduction pipeline is described (McGuire et al. 2020), but put briefly, the spectra in this data set cover the entirety of the X-, K-, and Ka-receiver bands with nearly continuous coverage from 8.0 to 11.6 GHz and 18.0 to 33.5 GHz (25.6 GHz of total bandwidth). All spectra have a uniform frequency resolution of 1.4 kHz (0.05–0.01 km/s in velocity) and an RMS noise of ~ 2 –20 mK, with the RMS gradually increasing toward higher frequency because of the lower integration times. Data reduction involved removal of RFI and artifacts, baseline continuum fitting, and flux calibration using complementary VLA observations of the source J0530+1331. Uncertainty from this flux calibration is estimated at $\sim 20\%$, and is factored into our statistical analysis described below (McGuire et al. 2020).

3. METHODS & ANALYSIS

3.1. Molecular spectroscopy

All the MPs and MCPs are prolate symmetric top molecules with C_{3v} symmetry, meaning their rotational energy states are defined by the total angular momentum state J in addition to its projection along the unique axis of rotation, denoted by the quantum number K . Depending on the value of J and K , symmetric top molecules will either exhibit A or E symmetry due to the nuclear spin on the methyl group; and since radiative and collisional transitions between these symmetry states are strictly limited, their relative populations can be far from the expected thermal distribution. Because of this, we treat transitions from non-degenerate (A_1 , A_2 symmetry) and doubly degenerate (E) levels separately by running independent MCMC fits. As such, we can compare the relative abundances of carbon chains in these energy states, similar to the separate treatment

Table 1. Spectroscopic properties of stacked CH₃C₇N lines covered by the GBT X-band receiver

Transitions		Symm.	Frequency	E_{up}	$S_{ij}\mu^2$	
$J' \rightarrow J''$	K	$F' \rightarrow F''$	(MHz)	(K)	(D ²)	
11 → 10	1	10 → 9	<i>E</i>	8243.824	9.92	355.325
		11 → 10	<i>E</i>	8243.824	9.92	389.482
		12 → 11	<i>E</i>	8243.836	9.92	426.877
	0	10 → 9	<i>A</i>	8243.851	2.37	358.286
		11 → 10	<i>A</i>	8243.859	2.37	392.727
		12 → 11	<i>A</i>	8243.865	2.37	430.435
12 → 11	1	11 → 10	<i>E</i>	8993.262	10.35	391.696
		12 → 11	<i>E</i>	8993.263	10.35	426.021
		13 → 12	<i>E</i>	8993.272	10.35	463.320
	0	11 → 10	<i>A</i>	8993.293	2.81	394.435
		12 → 11	<i>A</i>	8993.299	2.81	429.000
		13 → 12	<i>A</i>	8993.304	2.81	466.560
13 → 12	1	12 → 11	<i>E</i>	9742.699	10.82	428.012
		13 → 12	<i>E</i>	9742.700	10.82	462.478
		14 → 13	<i>E</i>	9742.708	10.82	499.692
	0	12 → 11	<i>A</i>	9742.733	3.27	430.560
		13 → 12	<i>A</i>	9742.739	3.27	465.231
		14 → 13	<i>A</i>	9742.743	3.27	502.666
14 → 13	1	13 → 12	<i>E</i>	10492.136	11.33	464.286
		14 → 13	<i>E</i>	10492.137	11.33	498.870
		15 → 14	<i>E</i>	10492.144	11.33	536.010
	0	13 → 12	<i>A</i>	10492.173	3.78	466.667
		14 → 13	<i>A</i>	10492.178	3.78	501.429
		15 → 14	<i>A</i>	10492.181	3.78	538.758
15 → 14	1	14 → 13	<i>E</i>	11241.572	11.86	500.524
		15 → 14	<i>E</i>	11241.573	11.86	535.211
		16 → 15	<i>E</i>	11241.579	11.86	572.284
	0	14 → 13	<i>A</i>	11241.612	4.32	502.759
		15 → 14	<i>A</i>	11241.616	4.32	537.600
		16 → 15	<i>A</i>	11241.619	4.32	574.839

NOTE—Only $K = 0$ and $K = 1$ are included here since they contribute the brightest transitions; however we still considered states as high as $K = 13$ in our MCMC model and stacking procedure. Similarly, lines ranging from $J' = 27$ to $J' = 44$ are covered by the GBT K- and Ka-bands and included in our analysis, but not shown here. For the full list of transitions used for CH₃C₇N and all other methyl carbon chains treated in this work, please refer to the linked Dataverse repository, [10.7910/DVN/K9HRCK](https://doi.org/10.7910/DVN/K9HRCK).

of the $K = 0$ and $K = 1$ components employed by Snyder et al. (2006) and Remijan et al. (2006).

For molecules with C_{3v} symmetry, the total statistical weight of rotational energy levels is the product of the typical J -degeneracy $g_J = 2J + 1$, the K -level degeneracy ($g_k = 1$ for $K = 0$ and $g_k = 2$ for $K \neq 0$), and the nuclear spin degeneracy g_I (Gordy & Cook 1984). The reduced statistical weight contributed by nuclear spin statistics of three identical hydrogen nuclei in a methyl group (each with spin $I = 1/2$) can be computed with the following:

$$g_I = \frac{1}{3} \frac{(4I^2 + 4I + 3)}{(2I + 1)^2}, \quad \text{for } K = 0, 3, 6, 9, \dots \quad (1)$$

$$g_I = \frac{1}{3} \frac{(4I^2 + 4I)}{(2I + 1)^2}, \quad \text{for } K \neq 0, 3, 6, 9, \dots \quad (2)$$

After combining all degeneracies, the states with A symmetry are weighted 2:1 relative to those with E symmetry, except in the case of $K = 0$ which is weighted equally because of the lower factor of g_k . The rotational constants for the largest MCPs and MPs were measured by Chen et al. (1998) and Travers et al. (1998b). To generate the spectroscopic data used for this work from these measurements, we used PGopher (Western 2017; Western & Billinghurst 2019), which is able to account for the necessary symmetry and statistical considerations. The input files and line lists for all six species are available on the Harvard DataVerse [10.7910/DVN/K9HRCK](https://dataverse.harvard.edu/dataset.xhtml?persistentId=doi:10.7910/DVN/K9HRCK).

As an example, Table 1 summarizes the spectroscopic properties of the rotational transitions of CH₃C₇N in X-band that were a part of this investigation. The transition quantum numbers, calculated rest frequencies (MHz), upper state energy level (K), transition line strengths $S(J, K)$ are presented. In the case of the MCPs, the nuclear spin on the nitrogen nucleus contributes hyperfine splitting to each rotational energy level.

Methyl acetylene (CH₃CCH) was not included in our analysis as it does not have any transitions covered by the GOTHAM survey. Similarly, although the fundamental transition of methyl cyanide (CH₃CN) is included in our spectra, a lack of additional lines prevents us from performing a full characterization of this molecule. For both CH₃CN and CH₃CCH, we refer to previous works studying these molecules in TMC-1 (e.g. Askne et al. (1984); Minh et al. (1993)), and instead base our analysis on the longer species.

3.2. MCMC modeling

In order to derive physical characteristics for the CH₃-polyyne and cyanopolyne species in TMC-1, we use the same Markov-Chain Monte Carlo (MCMC) model employed in previous publications from the GOTHAM collaboration McGuire et al. (2020); Xue et al. (2020); McCarthy et al. (2020). This procedure is discussed at length in Loomis et al. (2021), but we will summarize it here as well. In short, the MCMC model calculates probability distributions and covariances for parameters describing the physical and excitation conditions of a molecule in TMC-1. Based on recent observations performed with the 45 m telescope at Nobeyama Radio Observatory (Dobashi et al. 2018, 2019), as well as our data (Loomis et al. 2021), emission from molecules in TMC-1 toward the cyanopolyne peak display at least four

individual velocity components. In our current model, we make the assumption that the emission from each velocity component is cospatial, similar to the approach adopted in Loomis et al. (2021) for the cyanopolyynes. To summarize, the model describing a given methyl chain comprises a source size, four radial velocities, eight column densities and two excitation temperatures describing A/E components, and a linewidth parameter, giving a total of 16 parameters.

Line profile simulations were performed using MOLSIM (Lee & McGuire 2020). The MCMC simulations used wrapper functions in MOLSIM to ARVIZ (Kumar et al. 2019) and EMCEE (Foreman-Mackey et al. 2013); the former for analyzing the results of sampling, and the latter implements an affine-invariant MCMC sampler. As prior parameters, we used the marginalized posteriors from the corresponding cyanopolyne chain (e.g. HC₃N and CH₃C₃N). The prior distributions are approximated as normally distributed (i.e. $p(\theta) \sim N(\mu_\theta, \sigma_\theta)$ for parameter θ) with modifications to the variance σ_θ as to avoid overly constrictive/influential priors. Convergence of the MCMC was confirmed using standard diagnostics such as the Gelman & Rubin (1992) \hat{R} statistic, and by visually inspecting the posterior traces. With each of the six species studied in this work, we compute separate MCMC model fits for the *A* and *E* symmetry states so their relative populations could be derived directly through comparison of the posterior distributions.

3.3. Spectral line stacking and matched filter

Following the formalism of Loomis et al. (2018); Loomis et al. (2021), we perform a combined velocity stack and matched filter analysis in order to verify that the results of the MCMC model are consistent with the data, and determine the statistical significance of molecular detections. The first step involves a noise-weighted sum in velocity space of all expected transitions in our spectra, excluding any interloping transitions from known molecules in TMC-1; however, this was not necessary for any of the transitions in this analysis as there were no such interlopers. Next, the resulting composite spectrum is passed through a matched filter, using the best-fit parameters of the MCMC to create a model stacked spectrum. The impulse response of the matched filter, measured in signal-to-noise ratio σ , is a representation of how well the MCMC model reproduces GOTHAM spectra. Generally, we adopt a lower limit of 5σ as a threshold for confirmation of a molecule in TMC-1.

4. RESULTS & DISCUSSION

4.1. Column densities and physical characteristics

Figure 1 shows the stacked data, the stacked MCMC model, as well as the matched filter response of all the methyl carbon chains considered in this work. We clearly detect CH₃C₃N, CH₃C₅N, CH₃C₄H, and CH₃C₆H at high significance, and the model is able to fit all components (both velocity and hyperfine) of these molecules. In the case of CH₃C₇N, though no individual lines are present above the current noise level of the survey, the stacked emission in the top right of Figure 1 exhibits noteworthy signal. Furthermore, its matched filter has a central peak at 4.6σ , indicating evidence that this molecule is present in our data, and that the MCMC model converged to a set of parameters that reproduce its emission. The matched filter response is weaker than previous molecules that were found using this same method (Loomis et al. 2021; Lee et al. 2021; McGuire et al. 2021) and falls just below our desired 5.0σ threshold for a definitive discovery, but it is sufficient to consider a tentative detection and adopt the parameters of its fit in our analysis. For more information on this detection as it is indicated in the Bayesian fit to the spectra (prior to any stacking of emission lines), in Appendix A, we present corner plots illustrating the full results of the MCMC model for both CH₃C₇N and CH₃C₈H, and discuss the posterior distributions and covariances in the parameter spaces for each. In contrast to CH₃C₇N, CH₃C₈H shows a much higher degree of uncertainty in its fit, in addition to no signal in the stack nor its matched filter response (bottom-right panels of Fig. 1), so we therefore place upper limits on its column density.

A summary of parameters derived from the posterior distributions is provided in Table 2. Here, we note that the excitation temperatures of MPs (4.3 – 7.2 K) are systematically higher than those of the MCPs (3.4 – 3.9 K), which is in agreement with previous studies of these species in TMC-1 (Brotten et al. 1984; Askne et al. 1984; Snyder et al. 2006). However, one exception to this is seen for the *E* state of CH₃C₃N, which has $T_{ex} \sim 5.7$ K. At all derived excitation temperatures, we find that less than 4% of the total integrated line flux is contributed by transitions with $K > 1$. Furthermore, the population of the $K = 2$ state at these low temperatures is less than 1% for all detected chains, which is well within the uncertainty of our measured column densities. In that sense, although states up to $K = 13$ were considered, the column densities of the *A* and *E* components reported in Table 2 can be treated as equivalent to the column densities of the $K = 0$ and $K = 1$ components, respectively.

The total column densities (combining both *A* and *E* symmetries) decrease with increasing carbon chain

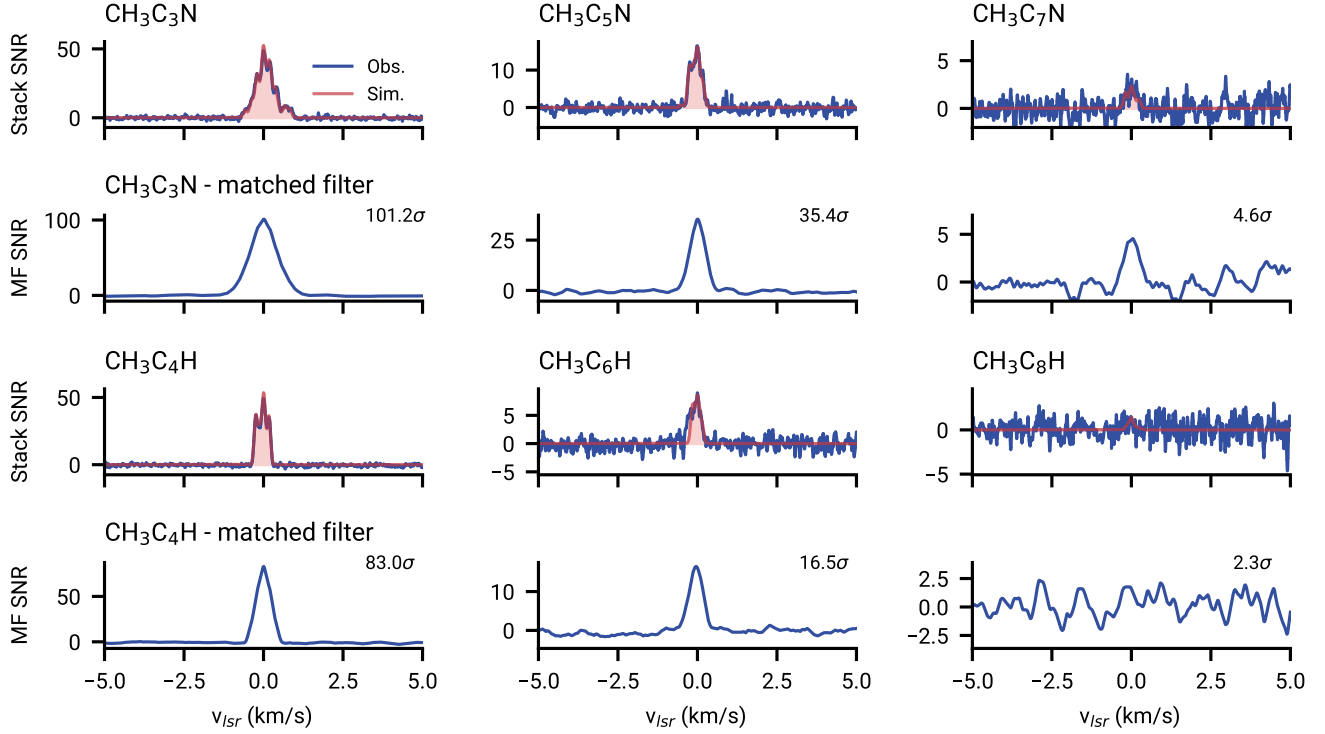


Figure 1. (First and third rows) Velocity stacks of the observational (blue) and MCMC simulated (red) spectra. The cross-correlation of the two velocity stacks for each molecule corresponds to the matched filter (MF) spectrum (second and fourth rows), which are shown in the second and fourth rows. Though the transitions belonging to *A* and *E* symmetry states were treated with separate MCMC fits, their results are combined here. The peak impulse response are annotated on the MF spectra.

Table 2. MCMC model results for all observed CH_3 -terminated carbon chains. Uncertainties are listed as the 95% confidence level.

Molecule	N_T (10^{11} cm^{-2})	N_A (10^{11} cm^{-2})	N_E (10^{11} cm^{-2})	T_{ex} (<i>A</i> sym.) (K)	T_{ex} (<i>E</i> sym.) (K)	Source Size "	<i>A/E</i> Ratio -
$\text{CH}_3\text{C}_3\text{N}$	8.66 (.46)	5.00 (.40)	3.66 (.24)	3.36 (.40)	5.70 (.26)	481.0 (8.7) ^a	1.37 (.15)
$\text{CH}_3\text{C}_5\text{N}$	2.86 (.30)	2.01 (.29)	0.85 (.07)	3.48 (.34)	3.97 (.48)	128.7 (4.9) ^b	2.40 (.40)
$\text{CH}_3\text{C}_7\text{N}$	0.86 (.19)	0.69 (.18)	0.17 (.06)	3.82 (.25)	3.90 (.44)	53.9 (1.0) ^c	4.20 (1.8)
$\text{CH}_3\text{C}_4\text{H}$	100.8 (5.7)	60.0 (5.0)	40.8 (2.8)	4.31 (.84)	5.50 (.37)	481.0 (8.6) ^a	1.46 (.15)
$\text{CH}_3\text{C}_6\text{H}$	10.4 (.72)	6.10 (.60)	4.30 (.40)	7.19 (1.2)	6.41 (1.1)	128.3 (4.8) ^b	1.41 (.20)
$\text{CH}_3\text{C}_8\text{H}$	< 0.98	< 0.8	< 0.18	-	-	-	-

^a HC_3N source size adopted as prior. See Loomis et al. (2021) for more details.

^b HC_5N source size adopted as prior.

^c HC_7N source size adopted as prior.

length, much like the similar linear cyanopolyynes (Loomis et al. 2021). This is shown pictorially in Figure 2, with a comparison to the column densities found by Remijan et al. (2006). There is small but notable disagreement (less than a factor of four) between the column densities we find and those derived in Remi-

jan et al. (2006). We attribute this discrepancy to the intrinsic line strengths (S_{ij}) adopted from our numerical treatment of these molecules (see Section 3.1) as they are factors of 2–3 larger than the analytic values employed in Remijan et al. (2006) and Snyder et al. (2006). Another important factor is that the column

densities we derive take into account decreasing source sizes, whereas previous studies of TMC-1 assume no effects due to beam dilution.

$\text{CH}_3\text{C}_7\text{N}$ has a total best-fit column density of $8.60 \pm 1.9 \times 10^{10} \text{ cm}^{-2}$, which matches well with the log-linear slope set by $\text{CH}_3\text{C}_3\text{N}$ and $\text{CH}_3\text{C}_5\text{N}$ (Fig. 2). Furthermore, this slope is very similar to that observed for the cyanopolyynes, and would imply the next chain ($\text{CH}_3\text{C}_9\text{N}$) to have a column density of about $3 \times 10^{10} \text{ cm}^{-2}$. To detect stacked emission from this molecule at such an abundance, the RMS noise of the survey would need to be reduced by at least factor of five. This would require several hundred more hours of integration time, primarily at lower frequencies (e.g. the GBT X-band receiver) because the brightest transitions of this molecule are simulated to be present in the 8–10 GHz range.

In contrast to the cyanopolyynes and MCPs, the MPs decrease in abundance at a much faster rate than the other carbon chains in TMC-1 (about 1 dex for each subsequent species). Furthermore, the upper limit we place on $\text{CH}_3\text{C}_8\text{H}$ appears to break the trend seen in the shorter methylpolyynes. A linear extrapolation on the column densities of $\text{CH}_3\text{C}_4\text{H}$ and $\text{CH}_3\text{C}_6\text{H}$ (the blue points in Fig. 2) would imply the next chain length has a column density $\sim 2 \times 10^{11} \text{ cm}^{-2}$, but in this case we would have detected emission from $\text{CH}_3\text{C}_8\text{H}$ at the sensitivity of our survey. Instead, it appears that the methylpolyynes experience a sharp drop-off in column density after $\text{CH}_3\text{C}_6\text{H}$, which indicates that the production of these carbon chains is severely hindered for these longer species.

A comparison to analogous linear species in TMC-1 is more difficult for the MPs, because the acetylene chains H_2C_{2n} have no dipole moment, and thus no rotational transition lines with which we could apply a similar analysis. However, the hydrocarbon radicals (C_{2n}H) do exhibit transitions in the radio/sub-mm and have been characterized in TMC-1 up to a chain length of eight by Brünken et al. (2007) (green points in Fig. 2). Here, it is apparent that those species also exhibit a non-linear decrease in column density after a carbon chain length of six. In other words, a similar ratio of $\frac{[\text{CH}_3\text{C}_8\text{H}]}{[\text{CH}_3\text{C}_6\text{H}]}$ to what is observed for $\frac{[\text{C}_8\text{H}]}{[\text{C}_6\text{H}]}$ would be in agreement with the upper limits we set in this work. This may suggest that similar chemical routes govern the abundances of both the MPs and the hydrocarbon radicals. However, since our upper limit on $\text{CH}_3\text{C}_8\text{H}$ is still very close to the log-linear extrapolated column density, it will be imperative to continue studying this molecule with future more sensitive data releases from GOTHAM survey to identify how steep this drop-off is, and how similar it is to the relative column density of C_8H .

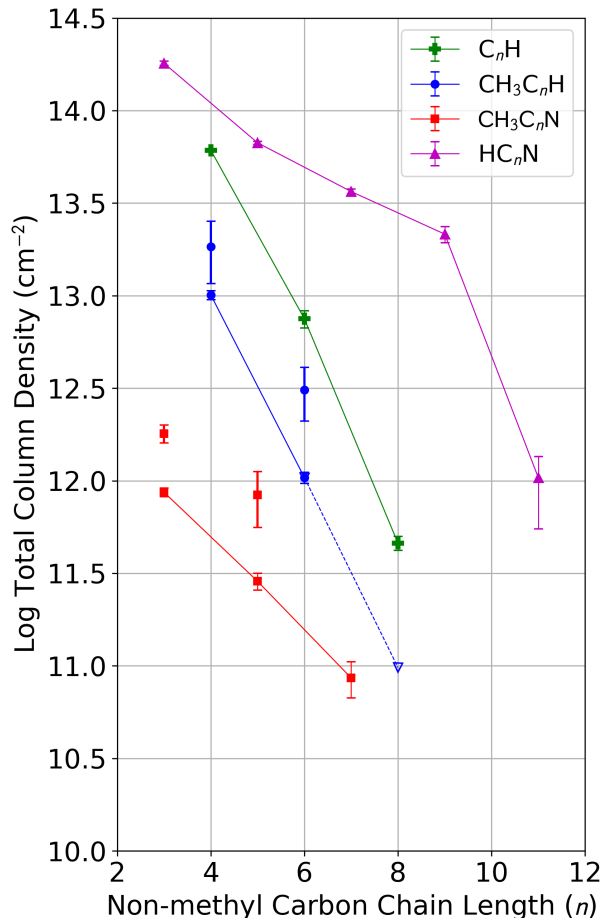


Figure 2. Derived total column densities of methyl-terminated carbon chains in TMC-1 as a function of chain length. Methylcyanopolyynes are shown in red while methylpolyynes are shown in blue. Contributions from the A and E symmetries of each species are summed, with their errors added in quadrature. $\text{CH}_3\text{C}_8\text{H}$ is denoted with a triangle as it is an upper limit. Results from Remijan et al. (2006) are overlaid in their respective colors with no connecting line. Additionally, column densities of the linear cyanopolyynes and hydrocarbons radicals published in Loomis et al. (2021) and Brünken et al. (2007) are shown in pink and green, respectively.

4.2. A/E symmetry state populations

Askne et al. (1984) found that in TMC-1, methyl acetylene (CH_3CCH) has about equal abundances of A and E symmetry states, which is not expected under LTE conditions and could indicate this molecule formed at a higher temperature. A similar result was found for $\text{CH}_3\text{C}_4\text{H}$ by Walmsley et al. (1984). In contrast, Minh et al. (1993) found that for CH_3CN in TMC-1, $N_E/N_A = 0.76 \pm 0.09$, which suggests that these states are equilibrated to the kinetic temperature. With the sensitivity and bandwidth of GOTHAM DR2, we are

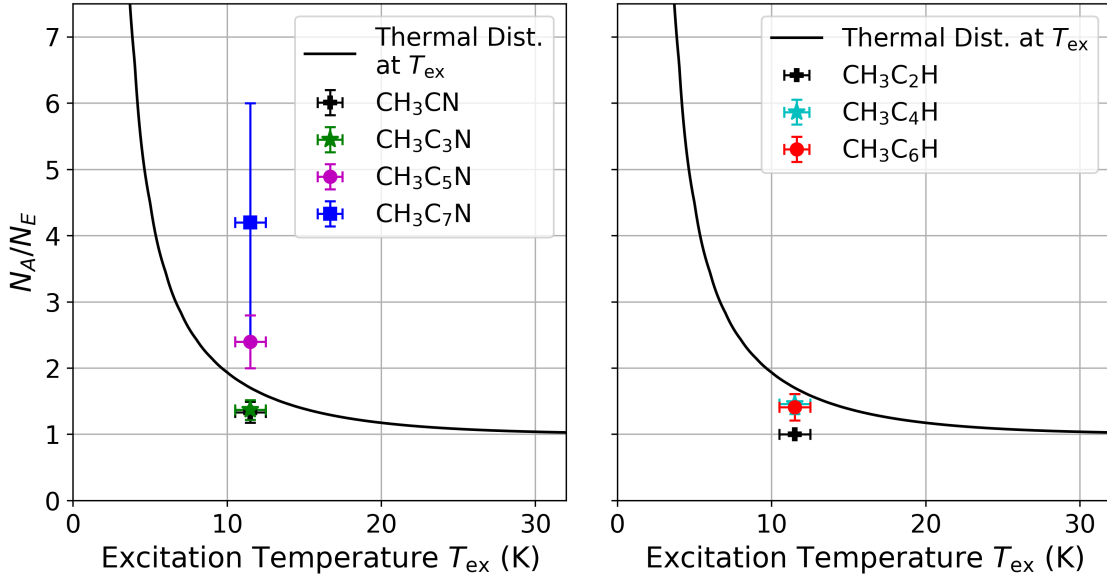


Figure 3. Column density ratios toward TMC-1 of *A* and *E* symmetry states for each of the chains studied in this work (colored points), as well as those derived for methyl cyanide and methyl acetylene by Minh et al. (1993) and Askne et al. (1984), respectively (black points). Also plotted in black is the expected ratio of these two populations if the molecules are thermalized to a Boltzmann distribution at a range of kinetic temperatures. The vertical error on the points represents the 95% confidence level from our MCMC modeling results, and the horizontal error bars denote the range of kinetic temperatures observed for gas phase molecules toward the CP region TMC-1 (Fehér et al. 2016).

able to revisit some of these population studies with a larger data set and expand them to the longer molecules $\text{CH}_3\text{C}_6\text{H}$, $\text{CH}_3\text{C}_3\text{N}$, $\text{CH}_3\text{C}_5\text{N}$, and $\text{CH}_3\text{C}_7\text{N}$. Because we performed separate MCMC analyses for the *A* and *E* states of each symmetric top carbon chain, their ratios can be computed directly and are shown in the last column of Table 2.

Figure 3 shows a comparison of all *A*/*E* ratios derived in this work plotted alongside the expected ratio in a thermalized distribution for a range of excitation temperatures. The gas phase kinetic temperature at the CP of TMC-1 has recently been placed at 11 ± 1.0 K by Fehér et al. (2016), so methyl chains with $A/E \approx 1.75$ can be considered as having equilibrated to this temperature.

For the MCPs (left plot in Fig. 3), we note that the *A*/*E* ratio increases for longer chain lengths, starting at a superthermal value of 1.33 for CH_3CN (as measured by Minh et al. (1993)) and reaching 4.2 ± 1.8 for $\text{CH}_3\text{C}_7\text{N}$ which corresponds to an excitation temperature of 6.1 ± 2 K, which is much lower than the kinetic temperature in TMC-1. In contrast, the MPs (right plot in Fig. 3) have nearly constant *A*/*E* ratios between 1.4 and 1.5. While this is only slightly smaller than the equilibrium value of 1.75, it is indicative that all MPs studied here have slightly larger *E* symmetry populations than what is expected given the physical conditions in TMC-1.

As noted in Section 3.1, both radiative and collisional interconversion between the *A* and *E* symmetry states are forbidden for both the MCPs and MPs (unless proton exchange collisions are non-negligible). Willacy et al. (1993) investigated the possibility that $E \rightarrow A$ conversion of CH_3CN occurs through *E*-state species adsorbing to and subsequently desorbing from grain surfaces in TMC-1. They found that this is an efficient process so long as the desorption rate is high enough. This may suggest that an important distinction may be happening in TMC-1. Highly exothermic reactions in the gas phase (e.g. dissociative recombination) may drive the formation of the MPs, forcing them into superthermal *A*/*E* distributions, where as the largest MCPs may preferentially form on (or stick to) the surfaces of dust grains. The non-thermal desorption of large complex molecules like the MCPs in TMC-1 has been a topic of numerous recent computation efforts (Garrod et al. 2007; Herbst & Cuppen 2006; Hoang & Tung 2019; Minissale et al. 2016; Shingledecker et al. 2021), but it is still difficult to say exactly how efficient this process is for the species explored here. The investigation of the potential bifurcation of the formation pathways between the MPs and the MCPs using astrochemical models might shed further light on this intriguing situation.

5. CHEMICAL MODELING OF METHYL CHAINS

To further explore the chemistry of methyl-terminated carbon chains in TMC-1, we utilized the adapted three-phase gas-grain chemical network model `nautilus v1.1` code (Ruaud et al. 2016) discussed in previous analysis of GOTHAM data, which has previously been used to successfully study the formation of carbon-chain molecules (Xue et al. 2020; McGuire et al. 2020; Shingledecker et al. 2021). The physical conditions of the model are equal to what has been previously used with this network ($T_{\text{gas}} = T_{\text{grain}} = 10$ K, $n_{\text{H}_2} = 2 \times 10^4 \text{ cm}^{-3}$, $A_V = 10$, and $\zeta_{\text{CR}} = 1.3 \times 10^{-17} \text{ s}^{-1}$; Hincelin et al. (2011)) as are the elemental abundances (Loomis et al. 2021). Based originally off of the KIDA network, the network already contained the formation of MCPs up to $n = 7$ and MPs up to $n = 6$. Here, we expanded on this to include the formation of $\text{CH}_3\text{C}_8\text{H}$, as well as additional reaction to better constrain the formation of the smaller members of this family.

To simulate the formation and destruction of $\text{CH}_3\text{C}_8\text{H}$, we utilized the analogous pathways for the existing network of $\text{CH}_3\text{C}_6\text{H}$, whose primary formation routes are from the dissociate recombination of C_7H_5^+ . As such, we expanded out the formation of C_9H_5^+ from ion-neutral reactions with semi-saturated carbon chains, whose rates were estimated using the Langevin formula (Woon & Herbst 2009). It should be noted that the rates for C_7H_5^+ and $\text{CH}_3\text{C}_6\text{H}$ are calculated using the Modified Arrhenius formula, which may result in some potential discrepancies between this and $\text{CH}_3\text{C}_8\text{H}$. As a source of destruction of C_9H_5^+ , we adapted existing dissociate recombination of similar cations. The rates and branching ratios C_9H_5^+ and C_7H_5^+ were estimated and updated, respectively, based on the dissociate recombination of C_5H_5^+ whose rates are taken from Herbst & Leung (1989) and branching ratios are discussed in detail on the KIDA website¹. In addition to dissociative recombination, C_nH_5^+ ions present in KIDA were also destroyed by reactions with anions. As such, the rates of the anion destruction of C_9H_5^+ were based off analogous rates estimated for C_7H_5^+ by Harada & Herbst (2008). Due to a lack of robust isomerization for large molecules within existing chemical networks, we only consider the C_7H_5^+ and C_9H_5^+ isomers with KIDA entries (i.e. $\text{CH}_3\text{C}_n\text{CH}_2^+$)

The analogous destruction of $\text{CH}_3\text{C}_6\text{H}$ was also adapted for $\text{CH}_3\text{C}_8\text{H}$. This included 1) dissociation due to photons and cosmic rays 2) ion-neutral reactions with abundant ions (i.e. H^+ , H_3^+ , C^+ , HCO^+ , and He^+) which were estimated with Langevin formula and

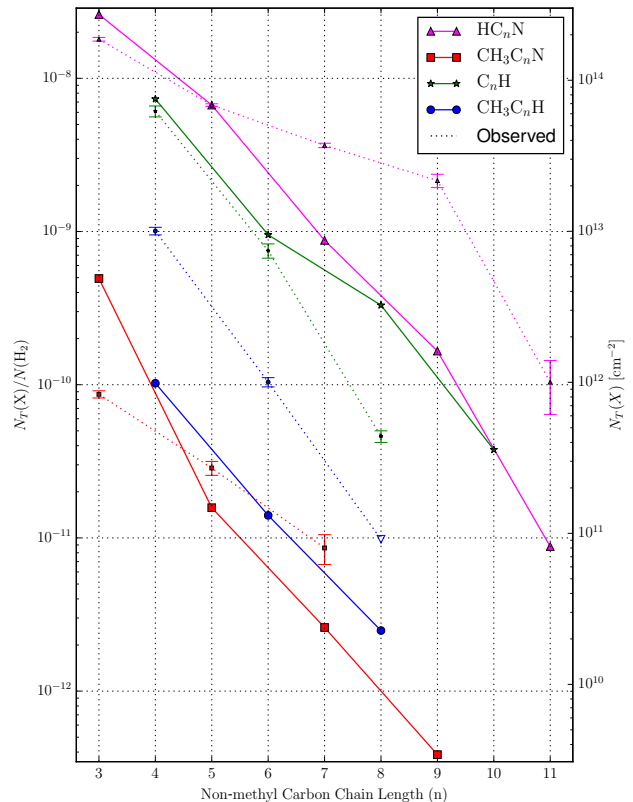


Figure 4. Simulated abundances and column densities of the four carbon chain families studied here at a model time of 2.5×10^5 years, with the same colors and markers as Figure 2. Observed values are shown as dotted lines and the $\text{CH}_3\text{C}_8\text{H}$ upper limit is denoted as an unfilled triangle.

3) reaction with elemental carbon to form C_{10}H_2 and H_2 . To properly study C_9H_5^+ , we also added in several neutral-neutral reactions to better account for the formation of C_5H_3 , a C_9H_5^+ -precursor, which were obtained originally from Hébrard et al. (2009). Finally, we included an additional formation pathway for the MPs by reactions of the C_{2n}H family with methane based on work by Quan & Herbst (2007) and formation of $\text{CH}_3\text{C}_4\text{H}$ from CH_3CHCH_2 by Berteloite et al. (2010).

For the MCPs, no additional reactions or rates were added from the KIDA network beyond the related adaptations from other recent molecular detections (e.g. the expanded semi-saturated carbon-chain networks for HC_4NC (Xue et al. 2020), $\text{C}_6\text{H}_5\text{CN}$ (Burkhardt et al. 2021a), $\text{H}_2\text{CCCHC}_3\text{N}$ (Shingledecker et al. 2021), and indene (Burkhardt et al. 2021b)).

The results of this model can be seen in Figure 4 at a time of 2.5×10^5 yrs, assuming a TMC-1 hydrogen column density of $N_{\text{H}_2} = 10^{22} \text{ cm}^{-2}$. At this time in the model, the simulated abundances of all studied species are within an order of magnitude of their observed val-

¹ <http://kida.astrophy.u-bordeaux.fr/datasheet/datasheet-2761-C5H5++e-V1.pdf>

ues. For the MCPs (solid red line in Fig. 4), the abundance of $\text{CH}_3\text{C}_3\text{N}$ is higher than the observed value, while the remainder of the family are somewhat below their observed value. As such, the log-linear trend is less well constrained here. The relative trend line was also fairly independent of time, with a slight increase of the longer chains at later times, as seen in Fig. A3. This is expected as longer chains typically have their peak abundance several 10^5 years after similar smaller chains, as seen by the cyanopolyynes (Loomis et al. 2021). The dominant formation pathways for the MCPs are the dissociative recombination of the $\text{C}_{n+1}\text{H}_4\text{N}^+$ ion family, which are in turn primarily produced by reactions between the cyanopolyynes and CH_3^+ , with minor contributions from $\text{C}_{n+1}\text{H}_3\text{N}^+$ and $\text{N} + \text{C}_{n+1}\text{H}_5^+$ after several 10^5 years. In particular, $\text{CH}_3\text{C}_3\text{N}$ has an additional production from $\text{H}_3\text{C}_4\text{N}^+ + \text{H}_2$ that may account for its deviation from the trendline of the rest of the MCP family. The MCPs are primarily destroyed by ion-neutral reactions with abundant ions (i.e. H^+ , H_3^+ , C^+ , HCO^+ , and He^+). The dependence on the cyanopolyynes (solid pink line in Fig. 4) is consistent with the similar observed abundance trends seen in Figure 2.

For the MPs (solid blue line in Fig. 4), the relative abundance trends of both the simulated and observed values are in good agreement at this time. This slope of this trend is also very consistent with the simulated abundance trend of the C_nH family (solid green line in Fig. 4). Within the general uncertainties of the source age of TMC-1 ($\sim 2\text{-}5 \times 10^5$ years), the abundance of $\text{CH}_3\text{C}_4\text{H}$ was found to be consistently in worst agreement with the observed values but improving at later times by a $\sim 60\%$ abundance increase, while the longer chains increased up to nearly an order of magnitude (See Fig. A3). As a result, the trend line was in less consistent agreement with the observed trend at later times, while reproducing the observed abundances better. Due to the overall depletion of $\text{CH}_3\text{C}_4\text{H}$, we have chosen this as a representative time as the simulated abundances are still within typical uncertainties for kinetic chemical models and we suspect the trend at this model time would remain consistent if a more efficient production is found either through new proposed pathways or improved reaction rate measurement/calculations. More generally, this strong dependence on the source age contrasts with other carbon chain families such as the cyanopolyynes and MCPs, whose observed trends are fairly consistent across the possible source ages of TMC-1.

The dominant formation route for the MPs are from the dissociative recombination of the $\text{C}_{n+1}\text{H}_5^+$ family, with a significant contribution from C_nH reactions

with methane after $\sim 10^5$ years. The $\text{C}_{n+1}\text{H}_5^+$ family are produced by various ion-neutral reactions, notably C_nH_2^+ with methane and C_{n+1}H_2 with C_2H_4^+ ($< 10^5$ years). These dominant pathways provide strength for the observed relation between the MPs and C_nH families. There is also an increased importance after 10^5 years of $\text{C}_4\text{H}_3^+ + \text{methane}$ for $\text{CH}_3\text{C}_4\text{H}$ and $\text{C}_3\text{H}_3 + \text{C}_4\text{H}_2$ for $\text{CH}_3\text{C}_6\text{H}$. MPs are mostly destroyed by ion-neutral reactions and reactions with carbon atoms.

Overall, the predictions of these chemical models are within an order of magnitude of agreement with the observed values of TMC-1, indicating that carbon chain chemistry can be fairly well understood. In addition, the observed MP trend line can be reproduced well and is also analogous to what is observed for C_nH . The estimated branching ratios and reaction rates still remain a major source of uncertainties in the models, which provide a strong motivation for further laboratory and theoretical studies. As discussed in Burkhardt et al. (2021b), detailed study of increasing larger molecules (e.g. molecules with 7+ heavy atoms and/or aromatic rings) will likely require a rigorous study of the formation of semi-saturated carbon chains that have historically been performed piecemeal. The recent expanded inventory of known carbon chains in TMC-1 will provide key constraints in this study.

6. CONCLUSIONS

We performed a rigorous, self-consistent study of methylpolyynes and methylcyanopolyynes in TMC-1 using the second data release of GOTHAM. Through MCMC modeling and matched filter analysis of stacked emission lines, we derived column densities, excitation temperatures, and A/E symmetry ratios for all previously found species, and discovered evidence for a new interstellar symmetric top, methylcyanotriacetylene ($\text{CH}_3\text{C}_7\text{N}$), at a confidence level of 4.6σ . We also searched for methyltetraacetylene ($\text{CH}_3\text{C}_8\text{H}$) in our spectra and place upper limits on its column density in TMC-1.

In our analysis, we found two important divisions between the different families of molecules explored in this work:

1. The column densities of methylcyanopolyynes decrease in a log-linear manner with increasing carbon chain length, and the slope of this trend is similar to the cyanopolyynes. In contrast, the methylpolyynes experience a drop-off in column density for species larger than $\text{CH}_3\text{C}_6\text{H}$ that is not consistent with the trend set by the smaller species.

- The A/E ratios of methylcyanopolyynes increase with carbon chain length, and are subthermal for the larger species. The detected methylpolyynes have systematically smaller A/E ratios which are not equilibrated to the kinetic temperature in TMC-1.

Given the structural similarity of the two classes of molecules, these dichotomies are striking and point to separate formation and carbon chain growth mechanisms in TMC-1. Whether these differences exist between the analogous cyanopolyynes (HC_{2n+1}N) and the pure hydrocarbon polyynes (H_2C_{2n}) is unclear, as the latter have no dipole moment. To understand this, future infrared observations of vibrational bands from these molecules toward TMC-1 would be instrumental in constraining their abundances and understanding their formation chemistry.

Finally, utilizing a gas-grain chemical network, we modeled the formation and destruction of CH_3 -terminated carbon chains in TMC-1. The model is able to reproduce our observed column densities to within

an order of magnitude, and we see very similar trends in the exponentially decreasing abundances with carbon chain length. However, we are not able to predict the observed drop-off in column density for $\text{CH}_3\text{C}_8\text{H}$ or C_8H using this model.

The results of this analysis offer important insights into the formation of carbon chain molecules in cold pre-stellar conditions, but it is important to note that many other families of unsaturated carbon chain species are known to form in TMC-1 (e.g. C_nO , C_nS , HC_nO). Similar in-depth analyses of these groups of molecules would be instrumental in improving our understanding the extent and efficiency of carbon chemistry in TMC-1.

We thank the reviewers for their thoughtful notes on this manuscript. The National Radio Astronomy Observatory is a facility of the National Science Foundation operated under cooperative agreement by Associated Universities, Inc. The Green Bank Observatory is a facility of the National Science Foundation operated under cooperative agreement by Associated Universities, Inc. M. A. S. acknowledges support from the Virginia Space Grant Consortium for this work.

REFERENCES

- Agúndez, M., Cernicharo, J., Quintana-Lacaci, G., et al. 2017, *A&A*, 601, A4, doi: [10.1051/0004-6361/201630274](https://doi.org/10.1051/0004-6361/201630274)
- Askne, J., Hoglund, B., Hjalmarsen, A., & Irvine, W. M. 1984, *A&A*, 130, 311
- Berteloite, C., Le Picard, S. D., Balucani, N., Canosa, A., & Sims, I. R. 2010, *Physical Chemistry Chemical Physics*, 12, 3666
- Broten, N. W., MacLeod, J. M., Avery, L. W., et al. 1984, *ApJL*, 276, L25, doi: [10.1086/184181](https://doi.org/10.1086/184181)
- Brünken, S., Gupta, H., Gottlieb, C. A., McCarthy, M. C., & Thaddeus, P. 2007, *ApJL*, 664, L43, doi: [10.1086/520703](https://doi.org/10.1086/520703)
- Burkhardt, A. M., Herbst, E., Kalenskii, S. V., et al. 2018, *Monthly Notices of the Royal Astronomical Society*, 474, 5068, doi: [10.1093/mnras/stx2972](https://doi.org/10.1093/mnras/stx2972)
- Burkhardt, A. M., Loomis, R. A., Shingledecker, C. N., et al. 2021a, *Nature Astronomy*, 5, 181, doi: [10.1038/s41550-020-01253-4](https://doi.org/10.1038/s41550-020-01253-4)
- Burkhardt, A. M., Long Kelvin Lee, K., Bryan Changala, P., et al. 2021b, *The Astrophysical Journal*, 913, L18, doi: [10.3847/2041-8213/abfd3a](https://doi.org/10.3847/2041-8213/abfd3a)
- Cabezas, C., Tercero, B., Agúndez, M., et al. 2021, *A&A*, 650, L9, doi: [10.1051/0004-6361/202141274](https://doi.org/10.1051/0004-6361/202141274)
- Cernicharo, J., Agúndez, M., Cabezas, C., et al. 2021, *A&A*, 649, L15, doi: [10.1051/0004-6361/202141156](https://doi.org/10.1051/0004-6361/202141156)
- Cernicharo, J., Marcelino, N., Agúndez, M., et al. 2020, *A&A*, 642, L17, doi: [10.1051/0004-6361/202039351](https://doi.org/10.1051/0004-6361/202039351)
- Chen, W., Grabow, J.-U., Travers, M., et al. 1998, *Journal of Molecular Spectroscopy*, 192, 1, doi: <https://doi.org/10.1006/jmsp.1998.7665>
- Chen, W., Grabow, J. U., Travers, M. J., et al. 1998, *Journal of Molecular Spectroscopy*, 192, 1, doi: [10.1006/jmsp.1998.7665](https://doi.org/10.1006/jmsp.1998.7665)
- Churchwell, E., Winnewisser, G., & Walmsley, C. M. 1978, *A&A*, 67, 139
- Dobashi, K., Shimoikura, T., Nakamura, F., et al. 2018, *The Astrophysical Journal*, 864, 82, doi: [10.3847/1538-4357/aad62f](https://doi.org/10.3847/1538-4357/aad62f)
- Dobashi, K., Shimoikura, T., Ochiai, T., et al. 2019, *The Astrophysical Journal*, 879, 88, doi: [10.3847/1538-4357/ab25f0](https://doi.org/10.3847/1538-4357/ab25f0)
- Fehér, O., Tóth, L. V., Ward-Thompson, D., et al. 2016, *A&A*, 590, A75, doi: [10.1051/0004-6361/201424385](https://doi.org/10.1051/0004-6361/201424385)
- Foreman-Mackey, D., Hogg, D. W., Lang, D., & Goodman, J. 2013, *Publications of the Astronomical Society of the Pacific*, 125, 306, doi: [10.1086/670067](https://doi.org/10.1086/670067)
- Garrod, R. T., Wakelam, V., & Herbst, E. 2007, *A&A*, 467, 1103, doi: [10.1051/0004-6361:20066704](https://doi.org/10.1051/0004-6361:20066704)
- Gelman, A., & Rubin, D. B. 1992, in *Bayesian Statistics* (Oxford University Press), 625 – 631

- Gordy, W., & Cook, R. 1984, *Microwave Molecular Spectra* (John Wiley & Sons)
- Harada, N., & Herbst, E. 2008, *The Astrophysical Journal*, 685, 272, doi: [10.1086/590468](https://doi.org/10.1086/590468)
- Hébrard, E., Dobrijevic, M., Pernot, P., et al. 2009, *Journal of Physical Chemistry A*, 113, 11227, doi: [10.1021/jp905524e](https://doi.org/10.1021/jp905524e)
- Herbst, E., & Cuppen, H. M. 2006, *Proceedings of the National Academy of Science*, 103, 12257, doi: [10.1073/pnas.0601556103](https://doi.org/10.1073/pnas.0601556103)
- Herbst, E., & Leung, C. M. 1989, *The Astrophysical Journal Supplement Series*, 69, 271, doi: [10.1086/191314](https://doi.org/10.1086/191314)
- Hincelin, U., Wakelam, V., Hersant, F., et al. 2011, *Astronomy & Astrophysics*, 530, A61, doi: [10.1051/0004-6361/201016328](https://doi.org/10.1051/0004-6361/201016328)
- Hoang, T., & Tung, N.-D. 2019, *ApJ*, 885, 125, doi: [10.3847/1538-4357/ab4810](https://doi.org/10.3847/1538-4357/ab4810)
- Irvine, W. M., Hoglund, B., Friberg, P., Askne, J., & Ellender, J. 1981, *ApJL*, 248, L113, doi: [10.1086/183637](https://doi.org/10.1086/183637)
- Kumar, R., Carroll, C., Hartikainen, A., & Martin, O. 2019, *Journal of Open Source Software*, 4, 1143, doi: [10.21105/joss.01143](https://doi.org/10.21105/joss.01143)
- Lee, K. L. K., & McGuire, B. A. 2020, *molsim*, Zenodo. <https://zenodo.org/record/4122749>
- Lee, K. L. K., Loomis, R. A., Burkhardt, A. M., et al. 2021, *ApJL*, 908, L11, doi: [10.3847/2041-8213/abdbb9](https://doi.org/10.3847/2041-8213/abdbb9)
- Loomis, R. A., Burkhardt, A. M., Shingledecker, C. N., et al. 2021, *Nature Astronomy*, 5, 188, doi: [10.1038/s41550-020-01261-4](https://doi.org/10.1038/s41550-020-01261-4)
- Loomis, R. A., Öberg, K. I., Andrews, S. M., et al. 2018, *The Astronomical Journal*, 155, 182, doi: [10.3847/1538-3881/aab604](https://doi.org/10.3847/1538-3881/aab604)
- Loren, R. B., Wootten, A., & Mundy, L. G. 1984, *ApJL*, 286, L23, doi: [10.1086/184377](https://doi.org/10.1086/184377)
- MacLeod, J. M., Avery, L. W., & Broten, N. W. 1984, *ApJL*, 282, L89, doi: [10.1086/184312](https://doi.org/10.1086/184312)
- Matthews, H. E., & Sears, T. J. 1983, *The Astrophysical Journal*, 272, 149, doi: [10.1086/161271](https://doi.org/10.1086/161271)
- McCarthy, M. C., Lee, K. L. K., Loomis, R. A., et al. 2020, *Nature Astronomy*, 1, doi: [10.1038/s41550-020-01213-y](https://doi.org/10.1038/s41550-020-01213-y)
- McGuire, B. A., Burkhardt, A. M., Kalenskii, S., et al. 2018, *Science*, 359, 202, doi: [10.1126/science.aao4890](https://doi.org/10.1126/science.aao4890)
- McGuire, B. A., Burkhardt, A. M., Loomis, R. A., et al. 2020, *The Astrophysical Journal Letters*, 900, L10, doi: [10.3847/2041-8213/aba632](https://doi.org/10.3847/2041-8213/aba632)
- McGuire, B. A., Loomis, R. A., Burkhardt, A. M., et al. 2021, *Science*, 371, 1265, doi: [10.1126/science.abb7535](https://doi.org/10.1126/science.abb7535)
- Mendoza, E., Bronfman, L., Duronea, N. U., et al. 2018, *ApJ*, 853, 152, doi: [10.3847/1538-4357/aaa1ec](https://doi.org/10.3847/1538-4357/aaa1ec)
- Minh, Y. C., Irvine, W. M., Ohishi, M., et al. 1993, *A&A*, 267, 229
- Minissale, M., Dulieu, F., Cazaux, S., & Hocuk, S. 2016, *A&A*, 585, A24, doi: [10.1051/0004-6361/201525981](https://doi.org/10.1051/0004-6361/201525981)
- Quan, D., & Herbst, E. 2007, *A&A*, 474, 521, doi: [10.1051/0004-6361:20078246](https://doi.org/10.1051/0004-6361:20078246)
- Remijan, A. J., Hollis, J. M., Snyder, L. E., Jewell, P. R., & Lovas, F. J. 2006, *ApJL*, 643, L37, doi: [10.1086/504918](https://doi.org/10.1086/504918)
- Ruaud, M., Wakelam, V., & Hersant, F. 2016, *Monthly Notice of the Royal Astronomical Society*, 459, 3756, doi: [10.1093/mnras/stw887](https://doi.org/10.1093/mnras/stw887)
- Shingledecker, C. N., Lee, K. L. K., Wandishin, J. T., et al. 2021, *A&A*, 652, L12, doi: [10.1051/0004-6361/202140698](https://doi.org/10.1051/0004-6361/202140698)
- Snyder, L. E., Hollis, J. M., Jewell, P. R., Lovas, F. J., & Remijan, A. 2006, *ApJ*, 647, 412, doi: [10.1086/505323](https://doi.org/10.1086/505323)
- Solomon, P. M., Jefferts, K. B., Penzias, A. A., & Wilson, R. W. 1971, *ApJL*, 168, L107, doi: [10.1086/180794](https://doi.org/10.1086/180794)
- Travers, M. J., Chen, W., Grabow, J. U., McCarthy, M. C., & Thaddeus, P. 1998a, *Journal of Molecular Spectroscopy*, 192, 12, doi: [10.1006/jmsp.1998.7666](https://doi.org/10.1006/jmsp.1998.7666)
- . 1998b, *Journal of Molecular Spectroscopy*, 192, 12, doi: [10.1006/jmsp.1998.7666](https://doi.org/10.1006/jmsp.1998.7666)
- Turner, B. E., Herbst, E., & Terzieva, R. 2000, *ApJS*, 126, 427, doi: [10.1086/313301](https://doi.org/10.1086/313301)
- Walmsley, C. M., Jewell, P. R., Snyder, L. E., & Winnemisser, G. 1984, *A&A*, 134, L11
- Western, C. M. 2017, *Journal of Quantitative Spectroscopy and Radiative Transfer*, 186, 221, doi: [10.1016/j.jqsrt.2016.04.010](https://doi.org/10.1016/j.jqsrt.2016.04.010)
- Western, C. M., & Billinghamurst, B. E. 2019, *Physical Chemistry Chemical Physics*, 21, 13986, doi: [10.1039/C8CP06493H](https://doi.org/10.1039/C8CP06493H)
- Willacy, K., Williams, D. A., & Minh, Y. C. 1993, *MNRAS*, 263, L40, doi: [10.1093/mnras/263.1.L40](https://doi.org/10.1093/mnras/263.1.L40)
- Woon, D. E., & Herbst, E. 2009, *The Astrophysical Journal Supplement Series*, 185, 273, doi: [10.1088/0067-0049/185/2/273](https://doi.org/10.1088/0067-0049/185/2/273)
- Xue, C., Willis, E. R., Loomis, R. A., et al. 2020, *The Astrophysical Journal Letters*, 900, L9, doi: [10.3847/2041-8213/aba631](https://doi.org/10.3847/2041-8213/aba631)

APPENDIX

A. MCMC POSTERIOR DISTRIBUTIONS

Figure A1 and A2 shows the MCMC posterior distributions for $\text{CH}_3\text{C}_7\text{N}$ and $\text{CH}_3\text{C}_8\text{H}$ respectively. Based on the off-diagonal heatmaps, we see that the majority of modeling parameters do not demonstrate significant covariance; those that do typically pertain to radial velocities and column densities of each velocity component, often those adjacent to one another in velocity and within the same symmetry group (i.e. E state column densities in neighboring velocity components). We do not expect significant covariance between the A/E states for both species, as they are by in large spectroscopically separate.

Regarding the treatment of source sizes, we observe quite different posteriors in comparison to the earlier work done by Loomis et al. (2021), which highlighted significant covariance between source sizes and column densities. We do not observe this for $\text{CH}_3\text{C}_7\text{N}$ most likely due to an overly constrained prior placed on the source size, and we likely underestimate its uncertainty and covariance. In the case of $\text{CH}_3\text{C}_8\text{H}$, we fixed the mean value of HC_7N Loomis et al. (2021), as we were interested in estimating upper limits to the column densities, and thus not shown in Figure A2.

Comparison of the posterior distributions for the column densities between $\text{CH}_3\text{C}_7\text{N}$ and $\text{CH}_3\text{C}_8\text{H}$ provides a margin for detection and non-detection cases. In the former, where the matched filtering shown in Figure 1 indicates a 4.6σ likelihood for $\text{CH}_3\text{C}_7\text{N}$, corroborating with smaller uncertainties in the column densities in comparison to $\text{CH}_3\text{C}_8\text{H}$, particularly for the first velocity component. We interpret this as a smaller range of column density values provide evidential support for the tentative detection of $\text{CH}_3\text{C}_7\text{N}$: even with the absence of individual lines, the likelihood-based sampling is able to place relatively large constraints on the possible values.

B. CHEMICAL MODEL TIME DEPENDENCE

Figure A3 shows the time-dependence of the simulated abundances within the `nautilus` chemical models in relation to the observed values. As it can be seen, the relative trend lines of these species can be quite time dependent, the time of peak abundance is strongly dependent on carbon chain length.

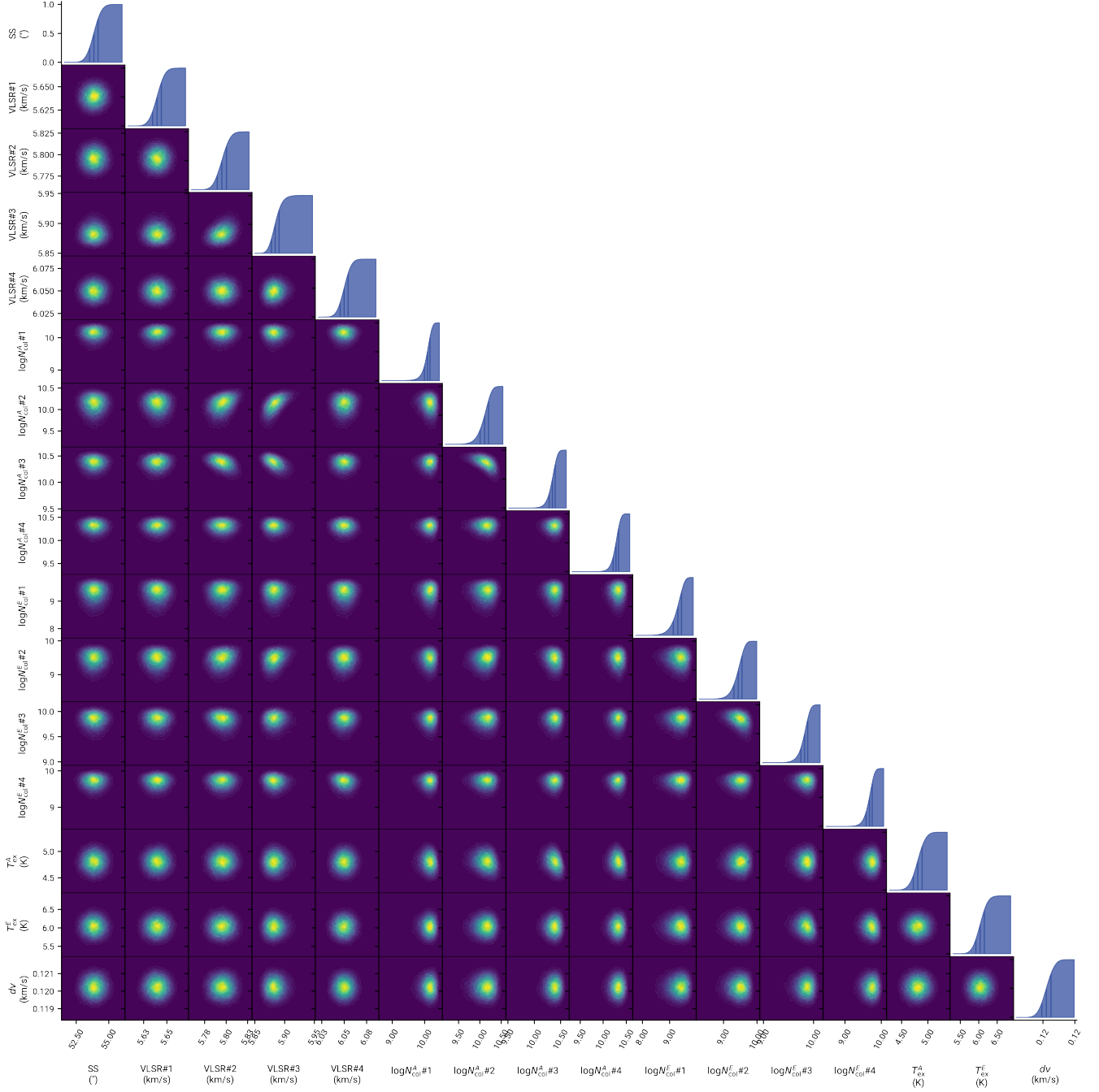


Figure A1. Corner plot for CH₃C₇N. The diagonal traces correspond to the marginalized, cumulative posterior distributions for each parameter, and off-diagonal heatmaps represent parameter covariances. Vertical lines in the cumulative distribution plots represent the first, second, and third quantiles.

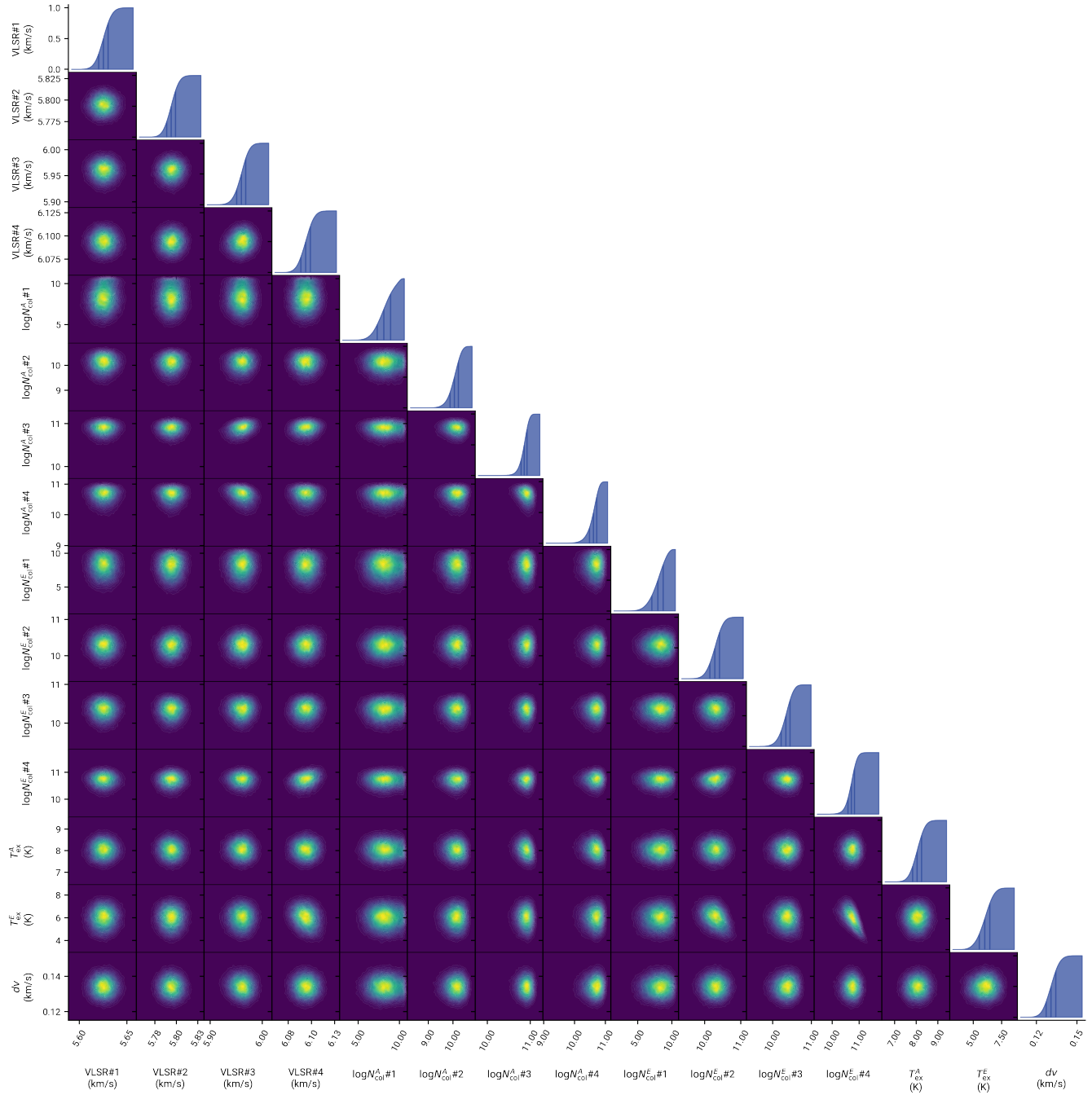


Figure A2. Corner plot for $\text{CH}_3\text{C}_8\text{H}$. The diagonal traces correspond to the marginalized, cumulative posterior distributions for each parameter, and off-diagonal heatmaps represent parameter covariances. Vertical lines in the cumulative distribution plots represent the first, second, and third quantiles.

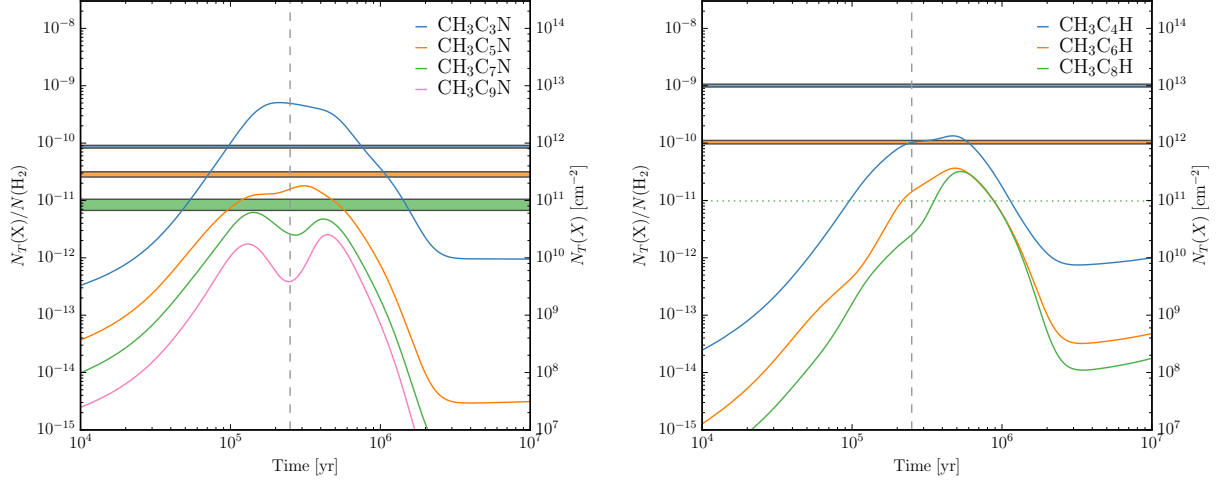


Figure A3. Simulated gas-phase abundance and column densities of the $\text{CH}_3\text{C}_n\text{N}$ (*left*) and $\text{CH}_3\text{C}_n\text{H}$ (*right*) families from *nautilus* chemical models in comparison to the observed values with uncertainties as a horizontal bars. The upper limit of the $\text{CH}_3\text{C}_8\text{H}$ is shown as green dotted line. The time used in Figure 4 is shown as a vertical dashed gray line.